УДК: 551.14:550.34+551.24(292.55) DOI: https://doi.org/10.24028/gj.v45i5.289104

The deep structure of the Zagros mountain system according to Taylor approximation seismic tomography data

T.O. Tsvetkova*, *O.B. Gintov, I.V. Bugaienko, L.M. Zaiets, 2023

S.I. Subbotin Institute of Geophysics of the National Academy of Sciences of Ukraine, Kyiv, Ukraine

Received 6 May 2023

The seismic tomographic model obtained by the Taylor approximation method provides new constraints on the Earth's crust and mantle structure beneath the Zagros mountain system at depths of 50—850 km. Based on structural geology and seismic tomography data, we divide the Zagros into Northwestern (Kirkuk, Lurestan, and Dezful regions) and Central (Kazerun and Fars regions) parts. The Central Zagros was formed due to subduction-collision tectonics, and the Northwestern Zagros was formed due to a collision-shear (transpression) tectonic process. Based on the 3D P-velocity model of the Zagros and its surrounding mantle, a high-velocity distal southeastern part of the Arabian Plate was established, subducting under the Central Zagros and the Iranian Plate, following the subduction of the Neotethys. This slab covers an area of 23—32°NL — 49—58°EL, i.e., the Bay of Bengal, the Central Zagros, and the southern part of the Iranian Plate. The maximum horizontal extent of the submerging part of the Arabian slab is 800—1100 km, and the maximum submersion depth is 450—500 km. A number of projections on the horizontal plane of the lines of intersection of the surface of the subducting Arabian Plate with horizontal sections of 50, 100, 200, 300, and 400 km were constructed. We obtained the direction of plate plunging, which in different areas varies from northern to northeastern 30—45°. In the Northwestern Zagros, according to the model, traces of subduction do not appear; however, right-lateral strike-slip deformations along the Main Recent Fault are visible and continue now in the crust. The difference in the types of deformation of the Northwestern and Central Zagros is most likely due to the features of the outlines of the eastern edge of the Arabian Plate and the complex nature of its movements. Analysis of earthquake mechanisms in 1977—2001 shows that the movement of the Arabian Plate could have occurred with frequent alternation in the S-N and N-E directions due to the alternation of spreading processes in the Gulf of Aden and the southeastern part of the Red Sea.

Key words: Zagros, Iranian plate, seismic tomography, mantle, subduction, collision.

Introduction. According to [Agard et al., 2011, p. 693], the Zagros region is «a long-lasting subduction system with changing boundary conditions makes the Zagros orogen an ideal natural laboratory for subduction processes». Many articles consider the mantle of the analyzed region of the Zagros using classical methods of seismic tomography [Hafkenscheid et al., 2006; Alinaghi et al., 2007; Chang et al., 2010; Paul et al., 2010; Simmons et al., 2011; Keshvari et al., 2011; Talebi et al., 2020, etc.].

In our paper, the velocity model of the Zagros mantle is analyzed by an alternative technique based on a Taylor approximation of the nonlinearity of a three-dimensional inverse kinematic problem. This method has been developed at the Institute of Geophy-

Citation: *Tsvetkova, T.O., Gintov, O.B., Bugaienko, I.V., & Zaiets, L.M.* (2023). The deep structure of the Zagros mountain system according to Taylor approximation seismic tomography data. *Geofizicheskiy Zhurnal*, *45*(5), 3—23. https://doi.org/10.24028/gj.v45i5.289104.

sics of the National Academy of Sciences of Ukraine since 1989 [Geyko, Tsvetkova, 1989]. The theoretical basis is described in [Geyko, 1997, 2004]. It has already been applied to studying the deep structure of mantle in many Eurasian regions such as the East-European Platform (Phennoscandia [Tsvetkova et al., 2010; Tsvetkova, Bugaenko, 2016], Sarmatia [Geyko et al., 2005, 2006]), Mediterranean [Geyko et al., 2007; Bugaenko et al., 2012; Gintov et al., 2016], South-Eastern Asia [Zaets, 2011; Zaets et al., 2012], Indochina [Zaets et al., 2009] and such well-known structures as the Ukrainian and Baltic Schields [Shumlyanskaya et al., 2014; Tsvetkova et al., 2016], Dnieper-Donets Depression [Tsvetkova et al., 2020], Trans-European suture zone [Gintov et al., 2022]. The method was applied to depth intervals from 50 km to 850—2500 km (depending on the observation system).

Before we turn to the results of studying the deep structure of the Zagros Orogenic Belt and the nearby area, we would like to outline the theoretical rationale behind the technique. It was published in English relatively long ago [Geyko, 2004] and is not easily found.

Theory. The seismic tomography method, as the method of solution of the inverse multidimensional seismic kinematic problem, develops in two directions: 1) the classical approach, which develops the ideas of V.G. Romanov, M.M. Lavrentiev [Lavrentiev, Romanov, 1966], Aki K., Christoffersson A., and Husebye E.S. [Aki et al., 1977], defining the relative correction to an *a priori* 1D reference model of velocity or slowness (the inverse value to the velocity); 2) the second approach represents the ideas related to the inversion of common travel-time fields, namely localization of velocity heterogeneities, and which represents the solution in the true velocities (the method of Taylor's approximation proposed by V.S. Geyko). The second approach is determined by the linearization of the eikonal equation associated with the expansion of slowness in a Taylor series in the vicinity of a given point. The results of using Taylor's approximation method in the common problem of travel-time inversion proposed by V.S. Geyko are given in [Geyko, 1997, 2004].

Applied to seismology, the general formulation of the problem is the following.

Let us assume that an area D is bounded by a boundary S in the Euclidean space R^3. Area D is the medium, where $n(x)$, $x=(x_1, x_2, x_3)$ is the slowness of the signal propagation. The time t of signal propagation from the point $x^0 \in S$ to the point $x^3 \in S$ is the solution of the eikonal equation:

$$\left|\nabla_x t\left(x^0, x^1\right)\right|^2 = n^2\left(x\right), \qquad (1)$$

on condition that $t\left(x^0,\ x^1\right) = 0\left(\left|x^0 - x^1\right|\right)$.

Here $\nabla_x = \left(\partial/\partial x_1\right) + \left(\partial/\partial x_2\right) + \left(\partial/\partial x_3\right)$ is the Hamilton operator. The rays along which the signal is distributed are the extremals of the functional

$$t\left(L\right) = \int\limits_{L\left(x^0, x^1\right)} n\left(x\right)\left|dx\right| , \qquad (2)$$

where $L(x^0,x^1)$ is the smooth curve that connects the points x^0 and x^1, and $\left|dx\right|$ is the Euclidean element of this arc. Let us represent the functional $t(x^0,x^1)$ according to these conditions as

$$\left(x^0, x^1\right) = \int\limits_{\gamma\left(x^0, x^1\right)} n\left(x\right)\left|dx\right| , \qquad (3)$$

where $\gamma(x^0, x^1)$ is the geodesic in the metric $dt = n\left(x\right)\left|dx\right|$.

Obtaining the slowness $n(x)$, $x=(x_1, x_2, x_3)$ from (3) is a nonlinear problem of travel-time inversion.

The method of Taylor's approximation assumes the following.

The Euclidean space R^3 of the variables (x, z), where $x=(x_1, x_2)$, and the axis z is directed downwards. Let the area $D = \left\{\left(x,\ z\right) : \left(\left|x\right| < \infty,\ 0 \le z < \infty\right)\right\}$ with the boundary S: $z=0$ be saturated by a medium, where $n(x, z)$ is the slowness (refraction coefficient) of P- or S-waves. We suppose that the function n is: a) positive, b) bounded, c) belongs to the space $C^2(D)$, d) decreases monotonously as the function of z variable, and e) such that

$$\sup_{-\infty<x^1,x^2<+\infty}\left\{\|n\|_{c^2(0,\infty)}\right\} >> \\ >> \sup_{0\le z<\infty}\left\{\|n\|_{c^2(-\infty,+\infty)\times c^2(-\infty,+\infty)}\right\}, \quad (4)$$

where $\|n\|$ is the norm n as the functions z on the left and is the norm n as the functions x on the right.

Let the refracted wave P or the S-wave propagate with the slowness $n(x, z)$ from the source $x^0 \in S$ to the receiver $x^1 \in S$ or vice versa along the geodesic $\gamma(x^0, x^1)$. Let $t(x^0, x^1)$ be the transmission time. We enter new variables $\xi(\xi^1, \xi^2)$, X, φ:

$$\xi_1 = \frac{\left(x_1^0 + x_1^1\right)}{2};\ \xi_2 = \frac{\left(x_2^0 + x_2^1\right)}{2};$$
$$X = \sqrt{\left(x_1^1 - x_1^0\right)^2 + \left(x_2^1 - x_2^0\right)^2};$$
$$\varphi = \text{arc tg}\ \frac{\left(x_2^1 - x_2^0\right)}{\left(x_1^1 - x_1^0\right)}.$$

The function $t(\xi, X, \varphi)$ is invariant concerning the reciprocal position of the source-receiver.

Let the function t of a variable ξ belong to the space $C^2(S)$ and be the continuous and single-valued function of variable X for each $\varphi \in [0, \pi)$. We agree that on the surface S, the wave front time of the wave disturbance $t(\xi, X, \varphi)$ generated by the refracted wave time travel field on the one hand and the slowness $n(x, z)$ on the other hand are connected by the eikonal equation:

$$\left|\nabla_\xi t(\xi, X)\right|^2 = n^2(x, z). \quad (5)$$

We assign the azimuth $\varphi \in [0, \pi)$. We approach the functions $n^2(x, z)$ and $t(\xi, X)$ on the variables x_1, x_2 and ξ_1, ξ_2 according to the Taylor series in the vicinity of the point ζ_1, ζ_2. We use the zero-order members. The Taylor equations are:

$$n^2(x, z) = n_\zeta^2(z) + R_1\left(n^2\right),$$
$$t(\xi, X) = t_\zeta(X) + R_2(t),$$

where $R(n^2)$ and $R(t)$ are the residual members of the Taylor's expansion. This expansion is correct if

$$R_2\left(n^2\right) = o\left(\left|x - \zeta\right|\right),\ x \to \zeta, \quad (6)$$
$$R_3(t) = o\left(\left|\xi - \zeta\right|\right),\ \xi \to \zeta. \quad (7)$$

If we assume that the remainder terms of the expansion of the functions n and t satisfy the introduced equations, i.e.,

$$R_1\left(n^2\right) = \left|\nabla R_3(t)\right|^2. \quad (8)$$

The V.S. Geyko's theorem is equitable [Geyko, 2004]: If the supposition (4), the equation (8), and the formulas (6) and (7) are true and the asymptotic estimations

$$\partial R_3(t)/\partial z = o\left(\left(\partial t_\zeta(X)/\partial z\right)^{-1}\right),\ \xi \to \zeta,$$

are valid, in the vicinity of point $\zeta \subset S$, the following Taylor's zero-order approximation of the eikonal equation (5) is correct:

$$\left(\frac{dt_\zeta(X)}{dz}\right)^2 = n^2{}_\zeta(z). \quad (9)$$

The equation (9) is the uniquely solvable equation concerning the function $n_\zeta(z)$ according to the travel-time curve (TTC) $t_\zeta(x)$ of the central middle point [Geyko, 1997].

Let us enfeeble the conditions on the slowness and determine the function $n(x, z)$ as 1) the positive function; 2) bounded; 3) related to the space $C(-\infty, +\infty)$ under variables (x, z); 4) as the function of variable z, as a) twice piecewise smooth; b) monotonically decreasing everywhere except the final number of low-velocity layers; 5) such that

$$\sup_{-\infty<x^1,x^2<+\infty}\left\{\|n\|c^1(0,\infty)\right\} \ge \\ \ge \sup_{0\le z<\infty}\left\{\|n\|c^1(-\infty,+\infty)\times c^1(-\infty,+\infty)\right\},$$

where, as before, $\|n\|$ is a norm $n(x, z)$ as the function z from the left and as the function x from the right.

Note that the area W as the definitional area $t(\xi, X, \varphi)$ of variable ξ coincides with the surface S.

Then, if the area $W = \bigcup_{i=1}^{m} W_i$, S_i corresponds to each area W_i.

Let us agree that in each area W_i, i=1; m function $t(\xi, X, \varphi$ a) belongs to the space $C^1(S_i)$ on variable ξ; b) continuous and single-valued as function X by each $\varphi\in[0,\pi)$. Each area W_i, I=1; m is between the boundaries $\partial w_i^{\uparrow}$ and $\partial w_i^{\downarrow}$, which we name the upper and the lower, respectively:

$$\partial w_i^{\downarrow} = X_i^{\downarrow}(\xi,\varphi) = \inf_{\xi}\left\{X:(\xi, X,\varphi)\in W_i\right\},$$

$$\partial w_i^{\uparrow} = X_i^{\uparrow}(\xi,\varphi) = \sup_{\xi}\left\{X:(\xi, X,\varphi)\in W_i\right\}.$$

Let us regulate S_i area and W_i consequently in an arbitrary point $\xi\in S_i$ so that $\partial W_j^{\downarrow} \le \partial W_{j+1}^{\downarrow}$ or $\partial W_{j\uparrow}^{\downarrow} \le \partial W_{j+1}^{\uparrow}$, $1\le j<i+1$. Let us insert a common numeration correct for a whole S. For each $\varphi\in[0,\pi)$, each $t(\xi, X)$ is determined single-valued, where $(\xi, X)\in W_i$ and $\xi\in S_i$, i=1; m. The areas W_i, i=1; m, are bounded by the surfaces:

$$X_i^{\downarrow}(\xi) = \inf_{\xi}\left\{X:(\xi, X)\in W_i\right\},$$

$$X_i^{\uparrow}(\xi) = \sup_{\xi}\left\{X:(\xi, X)\in W_i\right\}.$$

Thus, for each point $\xi\in\bigcup_{i=1}^{m} S_i$, there is an approximate equation

$$\frac{\partial\, t_\xi(X)}{\partial z} = n_\xi(z).$$

When we solve the variable problem of Lagrange by the following initial and boundary conditions t_0=0, t=t_ξ (X) and coming back to the variable ξ, we obtain

$$t_\xi(X) = \int_{\gamma_\xi(X)} n(z)\,dz\ , \qquad (10)$$

where $\xi\subseteq\bigcup_{i=1}^{m} S_i$.

Thus, (10) is the equation of the refracted wave travel time in 1D space with the refraction coefficient $n_\xi(z)$ along the ray path $\gamma_\xi(X)$ lying in the vertical plane x_2=ξ_2+(x_1−ξ_1) tan φ and symmetrical relative to the line x=ξ. For each fixed $\varphi\subseteq[0,\pi)$, the set $\{t_\xi(X)\}_{\varphi\subseteq S}$ is a Taylor's approximation of the initial travel-time field $t(\xi, X)$ obtained from the observations along the profiles with azimuth φ. It follows that the set

$$\left\{(X) = \int_{\gamma_\xi(X)} n_\xi(z)\,dz\right\}\left\{t_\xi\right\}_{\xi\subset S,\ \varphi\subset[0,\pi)}, \qquad (11)$$

is the full Taylor's approximation of central middle point time field $t(\xi, X,\varphi)$. If $\langle t\rangle$, $\langle\gamma\rangle$ and $\langle n\rangle$ are the averaged relative to φ on the set $[0,\pi)$ of the function t, γ, n, then the obtained approximation is the averaged Taylor's approximation. The analytical testing [Geyko, 1997] gives satisfactory results even under significant lateral velocity change.

Transferring from a curvilinear integral to a common one, we obtain the parametric imagination equivalent to the equation (10)

$$X_\xi(p) = 2p\int_0^{Z_\xi(p)} \frac{dz}{\sqrt{n_\xi{}^2(z) - p^2}},$$

$$T(p) = 2\int_0^{Z_\xi(p)} \frac{n_\xi{}^2(z)\,dz}{\sqrt{n_\xi{}^2(z) - p^2}},$$

where p=dt/dx, $Z(p)$=inf$\{z:n_\xi(z)\le p\}$. Curve $\Gamma_\xi\{(x,t):x=X_\xi(p),\ t=T_\xi(p),\ p\in(0,b_\xi)\}$, where b_ξ=sup$n_\xi(z)$ is a central middle point travel-time curve in the point ξ. The set $\{\Gamma_\xi\}_{\xi\in S,\varphi\in[0,\pi)}$ is a full Tailor's approximation of the true time fields $t(\xi, X, \varphi)$.

The transfer to the numerical inversion supposes the introduction of the monotonous non-decreasing function

$$H_\xi(u) = \mathrm{mes}\left\{z\ge 0 : n_\xi(z)\ge u\right\},\ u\ge 0,$$

and the inverse function to this

$$\tilde{n}_\xi(z) = \inf\left\{u\ge 0 : H_\xi(u)\le z\right\},\ z\ge 0.$$

Obviously, if $\tilde{n}_\xi(z) = n_\xi(z)$, i.e., waveguides are absent, then

$$X_\xi(p) = -2p\int_P^{b_\xi} \frac{dH_\xi(u)}{\sqrt{u^2 - p^2}};$$

$$T_\xi(p) = -2\int_P^{b_\xi} \frac{u^2 dH_\xi(u)}{\sqrt{u^2 - p^2}}.$$

According to [Geyko, 1997], the problem for the broad class of physically consistent velocities is solved uniquely relative to the

refraction coefficient $n_\xi(z)$ outside of the LVL and slowness distribution function

$$H^{\xi}_{L_k}(u) = \text{mes}\left\{z \subseteq L_k{}^{\xi} : n_\xi(z) \geq u\right\},\ u \geq 0,$$

that describes the set of solutions $\left\{n^*_\xi(z)\right\}$ in each LVL L^ξ_k, k=1; n.

The direct numerical inversion supposes the finite approximation of function $H_\xi(u)$ under the linear independent system $\{\psi_k\}$, k=1; m and the minimization solution in the metrics L^2. The conditional correctness of the inversion problem (11) is given in [Geyko, 2004], and the correctness of the inversion problem by Tikhonov is given in [Geyko, 2004].

In general, the numerical solution of the seismic tomography problem consists of three stages:

1. The construction of the central middle point travel-time field in coordinates (ξ, X, φ) and its analysis.

2. The construction of vertical cross-sections of the central middle point travel-time field.

3. The inversion of obtained cross-sections (the refracted travel time curve in the vertically heterogeneous medium).

The Taylor approximation general theory of the solution of the seismic tomography problem and methods of this approach are presented in [Geyko, 2004]. The numerical realization is given in [Geyko, Tsvetkova, 1989].

To conclude, the Taylor's approximation method proposed by Geyko for the solution of the seismic tomography problem has the following advantages:

– a more accurate approximation of nonlinearity;

– validity for fewer constraints imposed on a velocity function;

– no requirement for choosing a 1D referent model;

– is a correct problem by Tikhonov;

– reduces essentially the dimension of the numerical inverse problem.

The new seismic tomography method of arrival times permits us to obtain the optimal decision (the velocity model of the mantle) within the chosen basic interpretation model. The latter includes an *a priori* hypothesis, the theory, the numerical inverse algorithms, the velocity function parameterization, smoothing methods, and other regulation factors.

Data. The data of the *P*-waves first-arrival time at the station of the International Seismological Centre from 1964 to 2006, published

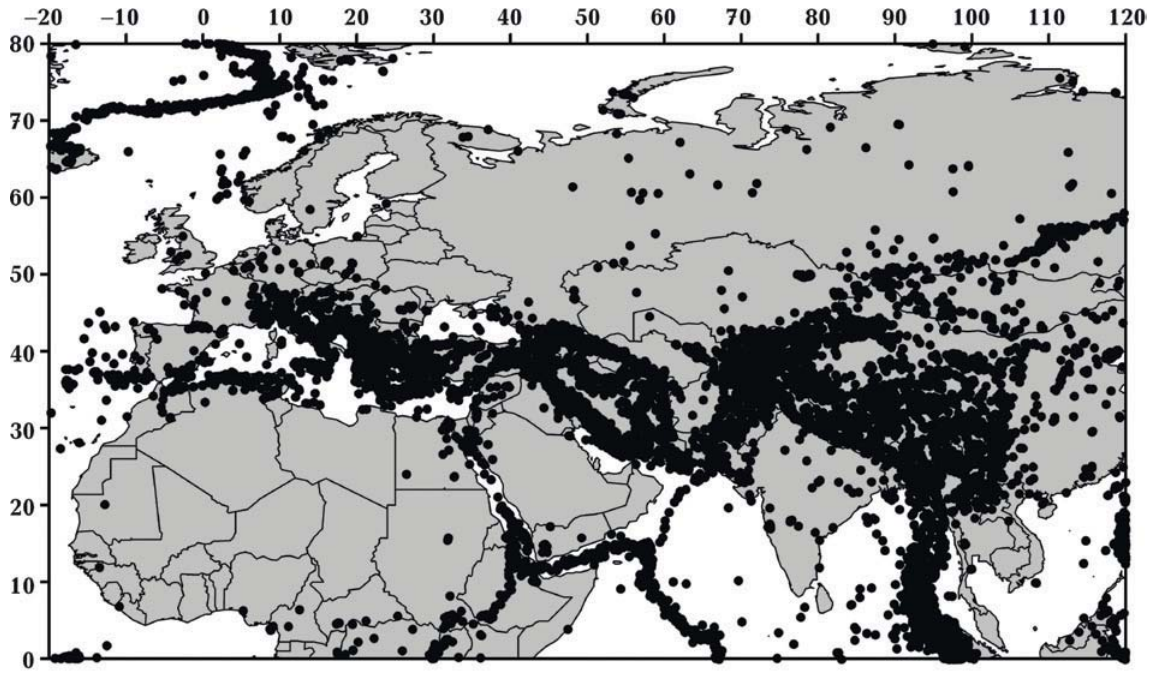

Fig. 1. Distribution of sources used in this study.

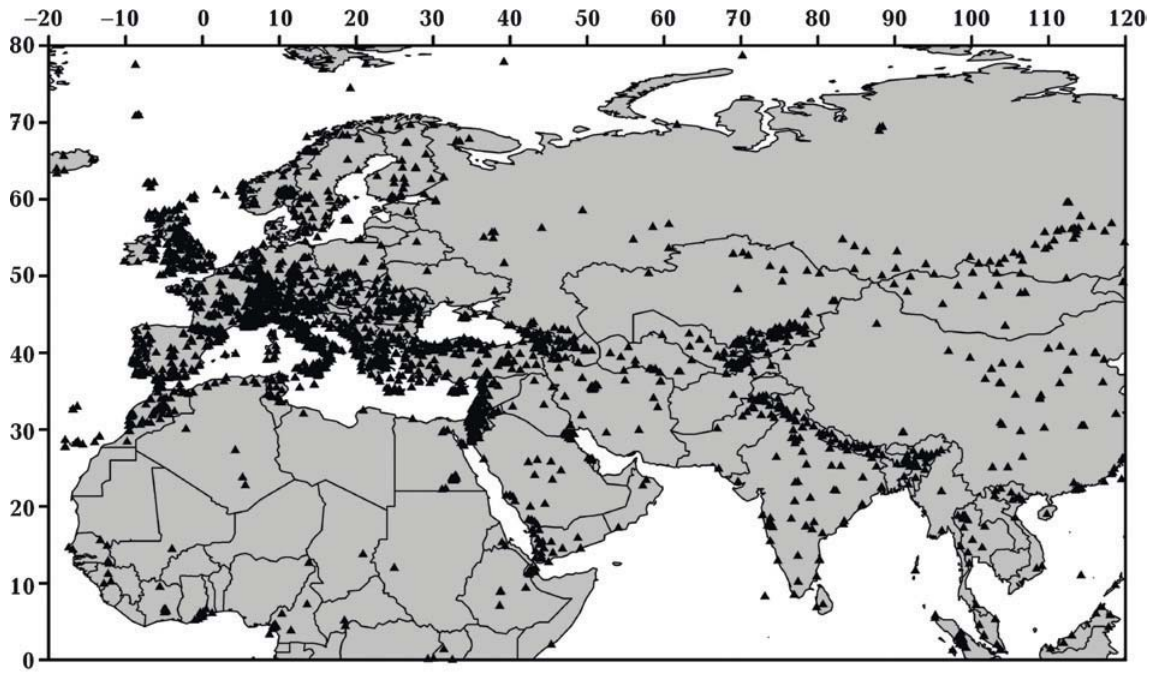

Fig. 2. Distribution of stations from the ISC catalogue used in this study.

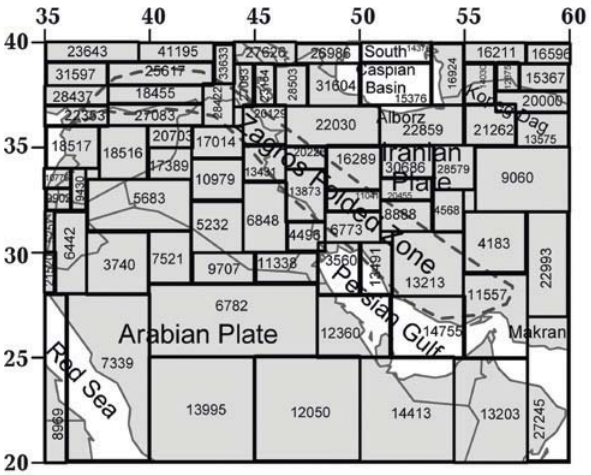

Fig. 3. The scheme of the cross-sections of the common travel-time fields of the Zagros region with the number of the points of the hodograph.

in the bulletins of the International Seismological Centre (ISC), are used as the primary data. The were selected earthquakes (Fig. 1) met the following requirements: 1) magnitude ≥4.5, 2) hypocenter depth ≤50 km, and 3) number of earthquake-detection stations ≥300. The considered ISC stations where the *P*-waves first-arrival times were registered are shown in Fig. 2. These earthquakes illuminate the mantle in the range of epi-central distance 0—105°.

The central middle point travel-time field was built to obtain the Zagros region's three-dimensional velocity model. 78 vertical cross-sections were obtained for the investigated region. The location of the obtained vertical cross-sections is shown in Fig. 3. The maximum of seismic rays for the Zagros region, related to the vertical cross-section of the common travel-time field (the number of the points of hodograph), is 41195 (to the north of Zagros Folded Zone). The minimum is 3740 (in the western part of the Arabian Plate). The correlation between the observed TTC related to one of 61 vertical cross-sections and the calculated theoretical TTC is shown in Fig. 4.

The calculation accuracy is 0.015 km/s, according to testing different parametrizations of the function $H_\xi(u)$. From that, the step has been chosen along the supposed isolines of velocity — 0.025 km/s. The numerical model is a 3D *P*-velocity dataset which is given on the analytical grid 0.25°×0.25°×25 km.

When visualizing the results, a generalized average velocity model for the mantle under the territory of Eurasia (Table) and its environ-

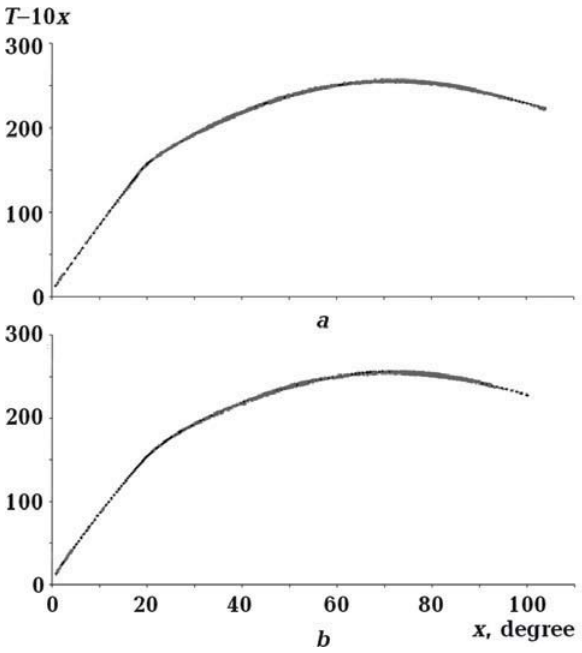

Fig. 4. Comparison of the experimental (gray) and theoretical (black) travel-time curve (TTC) in Zagros: *a* — under Lorestan, *b* — under Fars.

ment, obtained for a three-dimensional velocity model [Geyko et al., 1998], was used as a reference model: $V_{max}=\sup V(\varphi,\lambda,z)$, φ, $\lambda\in S$, $V_{min}=\inf V(\varphi, \lambda, z)$, φ, $\lambda\in S$,

$$V_{aver}(z)=z\left(\int_0^z \frac{d\zeta}{\sum(\zeta)}\iint_{s(\zeta)}\frac{d\varphi d\lambda}{V(\varphi,\lambda,\zeta)}\right)^{-1},$$

where $S(\zeta)$ is the section of the generalization area at the depth ζ and $\sum(\zeta)$ is its area in the coordinates φ, λ.

The deviations of true s velocities relative to the above generalized average velocity are presented as $\delta=V-V_{aver}$.

Then, if $\delta>0$ the velocities are increased, $\delta<0$ corresponds to reduced velocities, and $\delta=0$ — to the velocity boundary of the transition between these areas.

Horizontal sections of the mantle are presented in velocities with a depth step of 50 km, vertical ones are presented in 1° intervals as velocity discrepancies relative to the generalized model of the average velocity of Eurasia.

Zagros. General characteristics and an overview of geology. Zagros is a giant mountain belt spanning from the Arabian Plate and the Turkish-Iranian Plateau parallel to the Mesopotamian Plain and the Persian Gulf almost 1800 km from the East-Anatolian in the NW to the Oman system of fractures forming the Strait of Hormuz in the SE (Fig. 5). The width of the belt between the faults changes in the SE direction from 150 to

1D reference average *P*-velocity model of the upper mantle of the Eurasi

Depth, km	V_{min}, km/s	V_{max}, km/s	$V_{average}$, km/s
50	7.458	8.203	7.929
75	7.634	8.275	8.01
100	7.693	8.343	8.082
125	7.927	8.421	8.139
150	7.987	8.465	8.189
175	8.026	8.533	8.241
200	8.086	8.568	8.295
225	8.182	8.597	8.355
250	8.268	8.636	8.422
275	8.322	8.699	8.498
300	8.416	8.788	8.584
325	8.523	8.938	8.682
350	8.63	9.062	8.794
375	8.732	9.174	8.918
400	8.821	9.307	9.053
425	8.835	9.431	9.176
450	8.857	9.602	9.287
475	8.888	9.78	9.4
500	8.938	9.952	9.521
525	9.027	10.117	9.661
550	9.291	10.273	9.828
575	9.408	10.303	10.008
600	9.829	10.41	10.179
625	9.999	10.537	10.332
650	10.183	10.644	10.466
675	10.239	10.735	10.585
700	10.528	10.828	10.69
725	10.654	10.899	10.782
750	10.75	10.982	10.865
775	10.839	11.053	10.940
800	10.916	11.117	11.010
825	10.987	11.174	11.074
850	11.051	11.227	11.134

450 km. Previously [Wells, 1969; Falcon, 1974; Berberian, King, 1981], Zagros was divided into the Western (Kirkuk, Lorestan, and Dezful) and the Eastern (Fars), separated by the Kazerun submeridional system of fractures (fractures Borazjan, Kazerun, Kare Bas, and Sabz-Pushan) sometimes referred to as the Central Zagros. Later on [Agard et al., 2011; Mouthereau et al., 2012, etc.], this changed to NW Zagros (Lorestan) and Central Zagros (Fars), divided by Dezful Bay. We believe NW Zagros should also include Kirkuk and Dezful, and Central Zagros should also have the Kazerun region. These parts of the belt have distinctive kinematic characteristics, folding, and velocity features of the mantle (see below).

Zagros geology is described in many works [Wells, 1969; Falcon, 1974; Berberian, King, 1981; Alavi, 1994, 2007; Berberian, 1995; McQuarrie, 2004; Agard et al., 2006, 2011; Mouthereau et al., 2012, etc.] provide general overviews of the topic. Meanwhile, starting in the 1970s, the main focus has been on the character of the deformations connected with the convergence of the Arabian and Eurasian plates and the key role and time of subduction during convergence [Agard et al., 2006, 2011].

Zagros cross-section (from [Berberian, 1995], Fig. 6). To the SW, immediately after the Zagros Fore-Fold (ZFF, NE coast of the Persian Gulf) and the Zagros Foredeep (ZF) approximately 100 km wide, the belt is bordered by the Main Front Fault (MFF), followed by the so-called Zagros Simple Folded Belt (ZSFB) 150—200 km wide. Further to NE lies the High Zagros (HZ), separated from the previous region by the High Zagros Fault (HZF). At the NE, the belt is bordered by the Zagros Suture running to NW, which separates it from the Turkish-Iranian Plateau (in particular, from the Central Iran (Iranian Plate). The suture consists of two main fracture zones. In the NW it is the currently active zone of the dextral strike-slip fault over 1000 km long (Main Recent Fault, MRF) which in Central

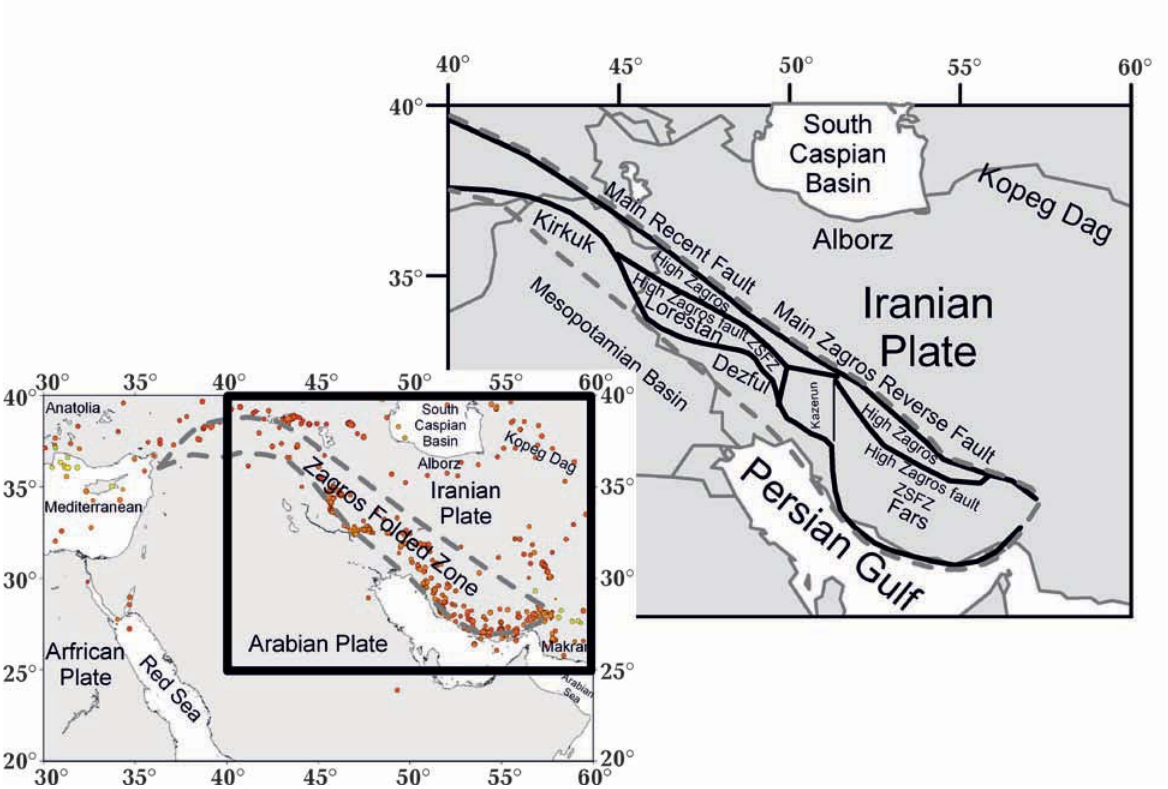

Fig. 5. Tectonic scheme of the study area with outlying hypocenters of strong earthquakes (with a magnitude of at least 5) for ten years (02.01.2011 to 02.01.2021) according to the data of the International Seismological Center [International…, 2023]. Borders of countries are marked with gray lines, discontinuous gray — Zagros Folded zone, black — the boundaries of tectonic structures.

Zagros assumes the submeridional direction and smoothly joins the system of dextral slip faults Dena and Kazerun-Borazjan (K-B). In the SE part of the suture, there lies the Main Zagros Thrust (MZT), also called Main Zagros Reverse Fault (MZRF), which is currently practically inactive. The SW part of the Turkish-Iranian Plateau 50—100 km wide touches and is partially thrust over Zagros Suture from NE is called the Sanandaj-Sirjan Zone (SSZ), of a rather unclear origin. In the north and east, the Turkish-Iranian Plateau borders the Lesser Caucasus, the Alborz mountains (south of the Caspian Sea), Kopeg Dag, and the Afghan Plateau.

Fold-fault tectonics, kinematics of Zagros, and paleotectonic reconstructions. Starting in the Late Precambrian — Early Paleozoic, the internal structure of the Zagros belt has undergone many transformations. During that time [Berberian, King, 1981; Cocks, Torsvik, 2006; Torsvik et al., 2012], the territory of the current Zagros, together with the Arabian Plate (AP) and the adjacent (from north and east, in the current coordinate system) terrains Taurida, Sanand, Alborz, and Lut (the foundation of the current Turkish-Iranian Plateau) were a single entity within Gondwana. It is thought [Berberian, King, 1981] that by the end of Precambrian, they had been cratonized (primary stage of compression) and comprised a continental massif (partly covered by a sea basin) and turned into a passive continental edge of the Arabian Plate washed by the Aegir Ocean or the Panthalassic Ocean. In its depressions, in the Late Precambrian — Early Cambrian, there were sedimented hormuz salt, red detritus, shallow-water carbonates, and salt-bearing shales. This plastic layer of a 1—2 km width played a noticeable role (as décollement and diapir tectonics) in further movements of layers and folds.

As transgression progressed in the Cambrian, Ordovician, and partly Silurian, the deepwater limestones and sandstones were laid upon the salt-bearing layer. In Devonian and Carboniferous, the continent's border was washed by a different ocean — Paleo-Tethys, yet there was a pause in the sediment accumulation; according to [Berberian, King, 1981], the region in question was dry, arid land during the Hercynian orogeny.

In Permian—Triassic, after [Berberian, King, 1981; Agard et al., 2011] or in Permian [Cocs, Torsvik, 2006] or Triassic [Khain, 2001], the spreading between the Arabian Plate and the abovementioned terrains created the Neo-Tethys Ocean. The synchronous enlargement of Neo-Tethys and narrowing of Paleo-Tethys, which subducted under Eurasia, led to a fairly quick movement of the terrains towards Eurasia. Thus, in the middle Jurassic [Berberian, King, 1981], Paleo-Tethys was closed off.

In the Neo-Tethys, the sediments of Mesozoic carbonates, sand-clay, and slate layers kept accumulating. However, starting from Cenozoic, only the continental sediments were laid onto the territory of Zagros and Iranian Plate, meaning that Neo-Tethys at the time (according to [Berberian, King, 1981] it was the border of Upper Cretaceous and the Paleocene — approximately 66 Ma; after [Khain, 2001; Mouthereau et al., 2012] it was Eocene) was also closed-off. Depen-

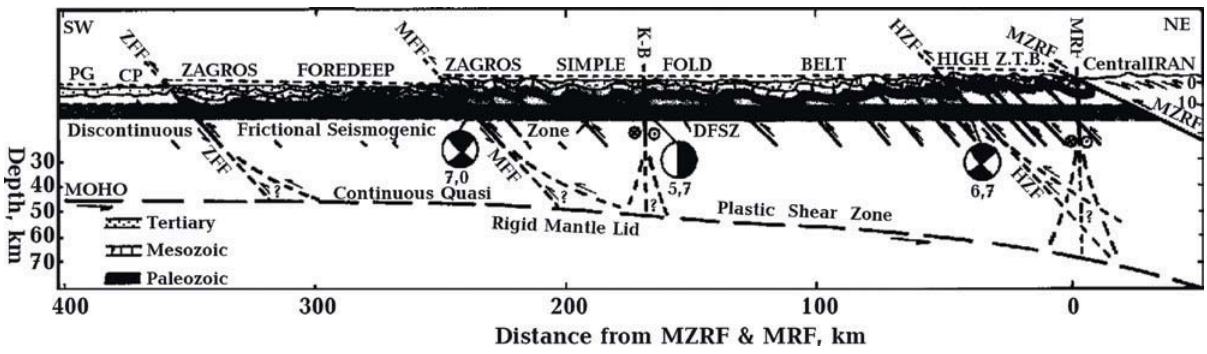

Fig. 6. Geological section of the contemporary Zagros crust along the Persian Gulf — Central Iran line [Berberian, 1995].

ding on the authors' views on the nature of the subduction-obduction processes, even later periods are offered as the Neo-Tethys closing times (Oligocene—Miocene [Allen et al., 2004; Chang et al., 2010; Agard et al., 2011]).

The overall thickness of the sediments accumulated over the time is up to 12 km [Mouthereau et al., 2012]. In the region of Zagros Suture and HZ in the upper part of the thickness, together with the tectonic mélange, there lie the layers of serpentinized ultrabazites Neyruz and Karmanshah (Upper Cretaceous — Paleocene, 66—56 Ma), as the allochthonous fragments of the Neo-Tethys ocean's lithosphere [Berberian, King, 1981; Golonka, 2004]. This is evidence of the beginning collision of the terrains with the Eurasian Plate and their gradual creation of the Turkish-Iranian Plateau. In principle, though, the collision process is still ongoing as the increasing compression and further rise of the mountains in some areas of Zagros and the Iranian Plate.

To generalize the most well-supported data, it is possible to conclude that the process of Neo-Tethys closing started with the oceanic crust subduction under the Iranian Plate in the Late Triassic [Xu et al., 2015] and lasted until the middle of the Paleogene. After that (35 Ma), the subduction was joined by the continental lithosphere of the Arabian Plate as its distal edge had negative buoyancy [Mouthereau et al., 2012]. This caused the thickening of the Zagros and Iranian Plate lithosphere and their uprise.

Approximately 10—15 million years later (Oligocene-Miocene), as the Red Sea and the Gulf of Aden opened under the action of the Afar Plume, the Arabian Plate was separated from the African and started moving to NNE. As a result, a dextral strike-slip fault began, under compression, along MRF and K-B. Meanwhile, along MZT, which together with MRF makes up an almost straight NE border of Zagros, there occurred mainly subperpendicular compression and thrust fault — underthrust fault. The change in kinematics of MRF and MZT and of the character of folding in the different parts of Zagros is usually explained by the effect of the system of submeridional dextral strike-slip faults of Kazerun, which re-orients the fold-fault structures [Talebian, Jackson, 2002, 2004; Authemayou et al., 2005; Lacombe et al., 2006].

However, a tectonophysical analysis of the mechanisms of earthquake sources (MES) of the Zagros region also allows for another interpretation of this phenomenon.

The article [Volfman et al., 2014] used the solutions for MES taken from the seismological catalogue of Harvard University (USA) in 1977—2001 (globalcmt.org/CMTsearch.html) for the Zagros region (25—40°NL and 40—60°EL). The selection includes 100 solutions for the mechanisms of mostly crustal focuses with M>4.0. Of them, 93 % solutions present two averaged fields of the subhorizontal tectonic compression in the following directions: field 1 (58 %) — submeridional 179°/5°, field 2 (35 %) — SW-NE 40°/9° (azimuth divided by the compression axis inclination). Also, MES of the slip fault (including reverse strike-slip fault) type comprise 46 % of cases, and the reverse strike type (slip fault — reverse strike), 47 %.

Under submeridional compression (Fig. 7, *a*), the majority of earthquakes with slip fault mechanisms are concentrated in the farthest NW part of Zagros, where the plains of sinistral strike-slip fault have the NE orientation because of the effect of displacements over the active East-Anatolian Fault. Over the rest of the area, the plains of slip fault acquire the Zagros orientation and the dextral character. Most earthquakes with MES of the reverse strike type are concentrated south of 33°NL. Here, the plains of the reverse strike have a sublatitudinal orientation and mostly southern fall.

Under the SW-NE compression (Fig. 7, *b*), almost all MES of either the slip or the thrust type are located (within the considered period) in an area south of 33°NL. The slips (not numerous) have the sublatitudinal orientation and sinistral type, and the thrusts are Zagros-oriented (perpendicular to the direction of compression) and have NE fall. All of this does not contradict the surface geological observations [Berberian, King, 1981; Berbe-

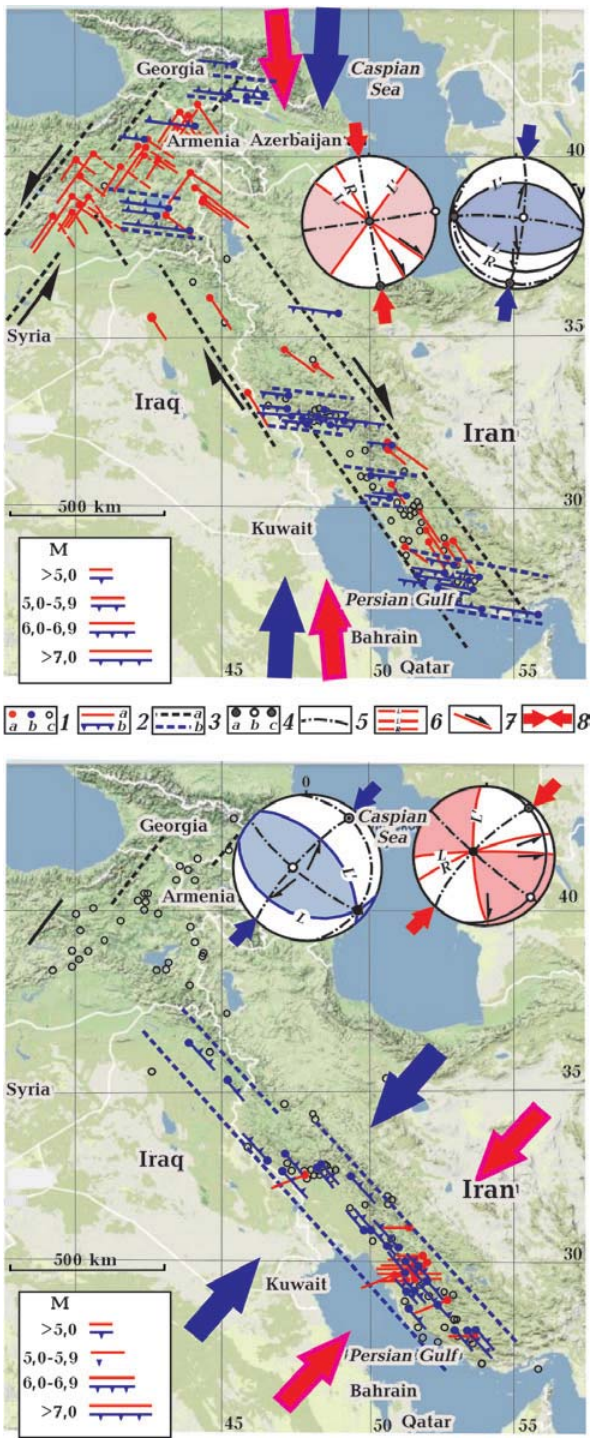

rian, 1995; Allen et al., 2004; Lacombe et al., 2006; Jahani et al., 2009; Mouthereau et al., 2012]. Notably, according to the seismological data of 1977—2001, the maximal numbers of earthquakes, which reflect either the submeridional or the SW-NE compression, are five years apart: 1988 (the former) and 1993 (the latter).

Thus, supposing that the tectono-seismic processes of 1977—2001 reflect the typical for Late Cenozoic Zagros geodynamic phenomena, it is fairly simple to hypothesize that the submeridional (practically meridional) subhorizontal compression and the no-less-clear SW-NE compression are consequences of the Arabian Plate moving in alternating directions. As a result of spreading processes in the Gulf of Aden and the western part of the Arabian Sea starting in the Miocene [Khain, 2001], the Plate moves northwards, and the maximum deformations (including destructive earthquakes) are concentrated on its narrow northern foreland.

The eastern ledge of the plate presses on the Central Zagros and the Iranian Plate, and there occur the maximum amount of sublatitudinal trust faults of northern vergence. The relaxation of the stresses of the submeridional thrust is followed by a spreading process of the SE part of the Red Sea which began in the Pliocene [Khain, 2001] and leads to the Arabian Plate moving to NE and the corresponding compression in the Central Zagros and the Iranian Plate. The complex nature of the folding structure of the Fars region [Berberian, King, 1981; Berberian, 1995; Authemayou et al., 2005; Lacombe et al., 2006; Tavakoli et al., 2008; Jahani et al., 2009], commonly explained by salt tectonics which has been going on since Paleozoic [Jahani et al., 2009], could

Fig. 7. Stereograms (lower hemisphere) of reverse-fault (black arrows) and strike-slip (gray arrows) earthquake source mechanisms, as well as the distribution of the corresponding sources in the Zagros territory: *a* — submeridional compression; *b* — NE-SW compression; *1* — earthquake sources (*a* — slip fault, *b* — reverse strike and thrust fault, *c* — others); *2* — lines of faults (*a* — slip fault, *b* — reverse strike and thrust fault), berghashes — the direction of the fall of faults; *3* — boundaries of seismogenic zones of slip fault and reverse strike type). *On stereograms*: *4* — projections of the main compression axes (*a* — maximum, *b* — minimum, *c* — intermediate); *5* — projections of the main planes; *6* — projections of the planes of supposed types of chips L, L', R; *7* — direction of displacement of the footwall of the fracture; maximum compression quadrants are white; *8* — the direction of regional compression, restored according to shear (red) and upthrust (blue) models. All structures are in the lower hemisphere. The inset in the lower left corner shows the earthquake magnitudes and the corresponding lengths of probable seismogenic ruptures.

also be caused by the superimposition of these two alternating processes of differently oriented compression.

The section in Fig. 6 demonstrates Zagros being compressed in the NE-SW direction. The author of the section M. Berberian [Berberian, 1995] delineates many «blind» faults — thrust faults, which disrupt the Paleozoic foundation in the ZF and ZSFB regions without continuing into the Mesozoic-Cenozoic cover. The latter responds to the compression with plicative deformations which are in many aspects connected to sliding along the Paleozoic salt-bearing shales layer. The main faults, such as ZFF, MFF, HZF, and MZRF (MZT), cross all of the crust and listrically continue in the Moho, which is why they are not shown on the seismotomographic model presented below.

The bending of Zagros sediment cover into compact (to the point of scale-like) folds of NW orientation points at the dextral strike-slip fault of the crust alongside MRF being no less important than the subduction process. The fault is oriented at ~40° to the current direction of movement of the Arabian Plate, and so the slip fault was accompanied by compression. Meanwhile, the dextral strike-slip fault could touch MZT as well when, after 35 Ma [Agard et al., 2011], the plates' convergence diverged from 45° by 20° NE and more.

Three-dimensional *P*-velocity model of Zagros mantle and its surroundings at a depth of 50—850 km. The papers [Chang et al., 2010; Paul et al., 2010; Agard et al., 2011; Simmons et al., 2011; Keshvari et al., 2011; Mouthereau et al., 2012, etc.] consider Early Miocene (when collision started) continental subduction, i.e., the subduction of the high-velocity distal edge of the Arabian Plate under the Iranian one. The Arabian slab then also took over the remains of the Neo-Tethys lithosphere. According to the data of [Keshvari et al., 2011], the velocity of *S*-waves within the distal part of the Arabian Plate to the depth of ~200—300 km is 6 % higher than in the Iranian Plate. A slab broke off NW of Zagros, and in the south (Central Zagros), the uninterrupted Arabian Plate moved over 500 km under the SSZ and central Iran [Mouthereau et al., 2012].

Agard et al. [2011] also provide interesting data about the change in the direction of convergence of the Arabian and Eurasian Plates during the last 150 Ma. According to them, in the Early Cretaceous (140—115 Ma), the convergence occurred in the sublatitudinal direction (85° NE); during 115—80 Ma, it gradually changed to the normal 45°NE, and since 80 Ma, it has gradually acquired the direction of 5°NE.

Seismic tomographic materials after the method of V.S. Geyko using the Taylor approximation series we provide in our work are consistent with the data of [Agard et al., 2011; Mouthereau et al., 2012]. However, they allow a more precise delineation of the sinking slabs and the mantle's general velocity division down to 850 km. Unfortunately, the unstable orientation of the convergence zone of the Arabian and Eurasian Plates does not allow the precise age and sequence of subduction processes presented on the vertical (longitudinal and latitudinal) sections. It is only clear that all the sections of the velocity model of the mantle reflect, first of all, the latest (until the present time) changes in the velocity structure of the region's mantle. Also, one cannot deny the possibility that traces of earlier Mesozoic-Cenozoic processes could also be preserved (see, e.g. [Chang et al., 2010]) and complicate the general direction of the slab's sinking and their outlines.

Horizontal sections of the mantle. The crust in the convergence area of the Arabian Plate and the margins of Eurasia is not generally over 50 km thick, and only in the narrow SSZ zone can it be more than 70 km [Mouthereau et al., 2012]. In the sections of our model, the mantle is shown in the depth interval of 50 to 750 km with velocities V_P (Fig. 8). The yellow color shows the middle-for-Eurasia velocity for every depth (see Table). The mantle under Zagros has velocity parameters near almost the whole Mediterranean fold belt [Geyko et al., 2007; Bugaenko et al., 2012; Gintov et al., 2016]; within it, from 50 to 225—450 km deep, the mantle is characterized mostly by lower velocities; deeper, there occurs a velocity inversion (to higher values) down to 650 km, below which the mantle again has lower ve-

locity. The pattern does not contradict other works such as [Artemieva, 2009, 2019].

As for Zagros proper and the Iranian Plate and the NE distal part of the Arabian Plate which are adjacent to it, one has to consider two parts of the mantle that practically follow the tectonic division: the NW (NW Zagros) and SE (Central Zagros). The division is seen throughout the whole considered depth in the area of 32.5°NL, 50.0°EL at the highest mountain in Zagros — the Zard-Kuh Mountain.

At a depth of 50 km, both parts of Zagros are low-velocity. However, there are already signs of the introduction of the high-velocity distal regions of the Arabian Plate into the highest part of the Zagros mantle. That is, already at this depth, one can see the surface of the subducting slab, which on deeper sections (down to 300—500 km) moves ever northwards and eastwards for over a thousand kilometers (which is well in line with the horizontal sections of V_P velocities presented in [Alinaghi et al., 2007]. At a depth of 100—150 km, the distal parts of the Arabian Plate mantle under Zagros belong to a practically single high-velocity region divided only within the described section area. This area is limited by the NE area of high gradients, which points at a clear boundary of the upper boundary of the slab sinking below the Iranian Plate. However, already starting at 200 km and down to the inversion zone, there are seen under most of the NW Zagros reduced velocities V_P, which could also be evidence of the absence of a subduction process or the slab breaking off.

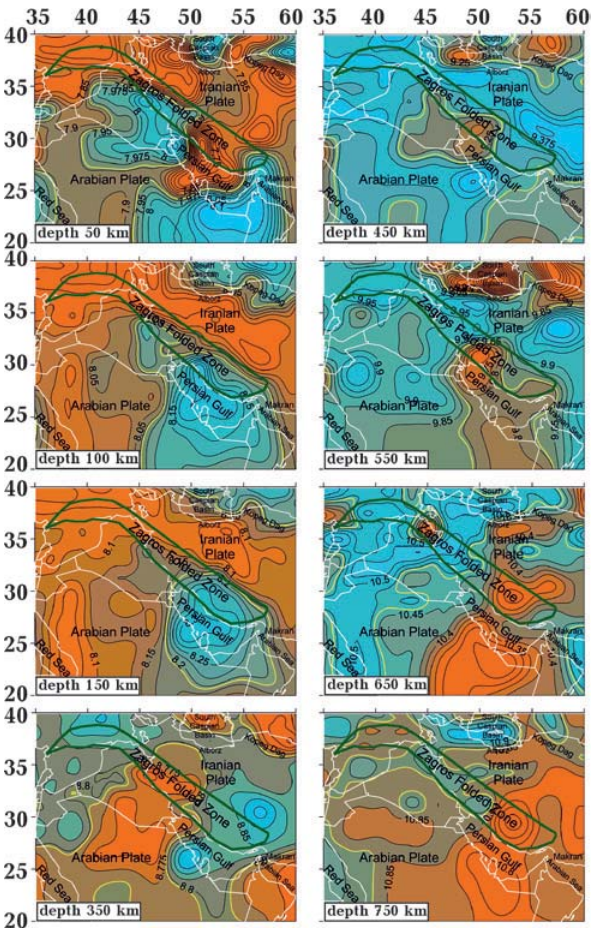

Fig. 8. Horizontal sections of the 3D *P*-velocity model of the mantle of the Zagros Folded Zone and its surroundings at 50, 100, 150, 350, 450, 550, 650, and 750 km depths. The green line shows the Zagros Folded Zone and the white line shows the borders of countries.

Generally, starting at 150 km depth, Central Zagros and the southern part of the Iranian Plate are segregated into an isometric high-velocity area reflecting the Arabian Plate's subduction under these structures as seen from the vertical sections. The epicenter of the high-velocity area at a depth of 150 km lies at 27°NL, 53°EL, and at a depth of 450 km at 30°NL, 57°EL (~600 km to NE). And while at a depth of 150 km and above, it lies within the Arabian Plate, below 250 km, it lies under the Iranian one.

Vertical sections of the mantle. The longitudinal and latitudinal sections (Fig. 9, 10) present the obtained velocity model of the Zagros mantle in more detail. They reflect the mantle's structure down to 850 km. The most interesting are the high-velocity layers sinking under Zagros and partly under the Iranian Plate northwards on the longitudinal (sections 49—58°EL in the area from 23—25° to 32—33°NL) and eastwards on the latitudinal sections (sections 28—32°NL in the area from 49° to 57—58°EL). The layers are 200—300 km thick, 800—1100 km long (as horizontally projected onto the surface), and lie 300 to 500 km deep.

Therefore, in this case, we have a high-velocity lithosphere sinking due to subduction and most probably belonging to the distal part of the Arabian Plate. Also, on the longitu-

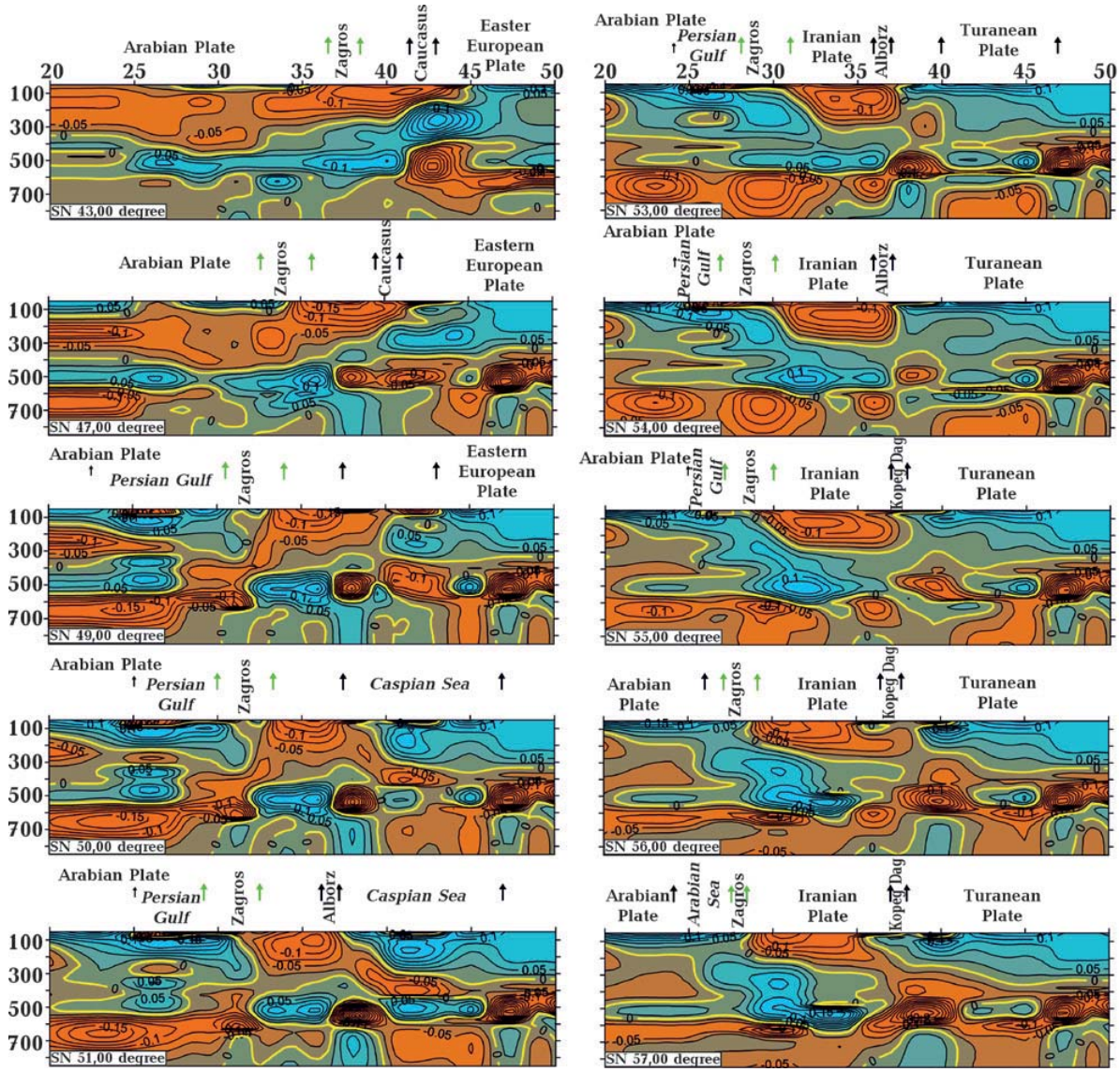

Fig. 9. Vertical meridional sections of the 3D *P*-velocity model of the mantle of the Zagros Folded Zone and its surroundings (43°, 47°, 49°, 50°, 51°, 53°, 54°, 55°, 56°, 57° EL). Black arrows mark the boundaries of tectonic structures, green — Zagros.

dinal sections of 43—57°EL, one can see high-velocity inclined layers that sink southwards from the Scythian and Turanian Plates of the East-European Platform.

The vertical and horizontal sections showed the positions of the distal part of the Arabian Plate, which has high velocity and provided the subduction. On the horizontal section at 50 km and the sections of 28—34°NL its outermost SW part passes to 40°EL, and in the south (23°NL section) to 45°EL, so the distance from the W to the S margins of the high-velocity part of the plate to the beginning of the subduction is 600—900 km. We determine the place of subduction's start from the areas of transition from the horizontal to the inclined position of the slab.

On the sections 48—51°EL in the region of 32.5°NL, one can see the mantle's border under the NW and Central Zagros (see Fig. 5), which is recognized as subvertical velocity inhomogeneities (between the areas of increased and reduced velocities) throughout the whole depth profile.

On all vertical sections within the areas where the Arabian slab starts sinking, its

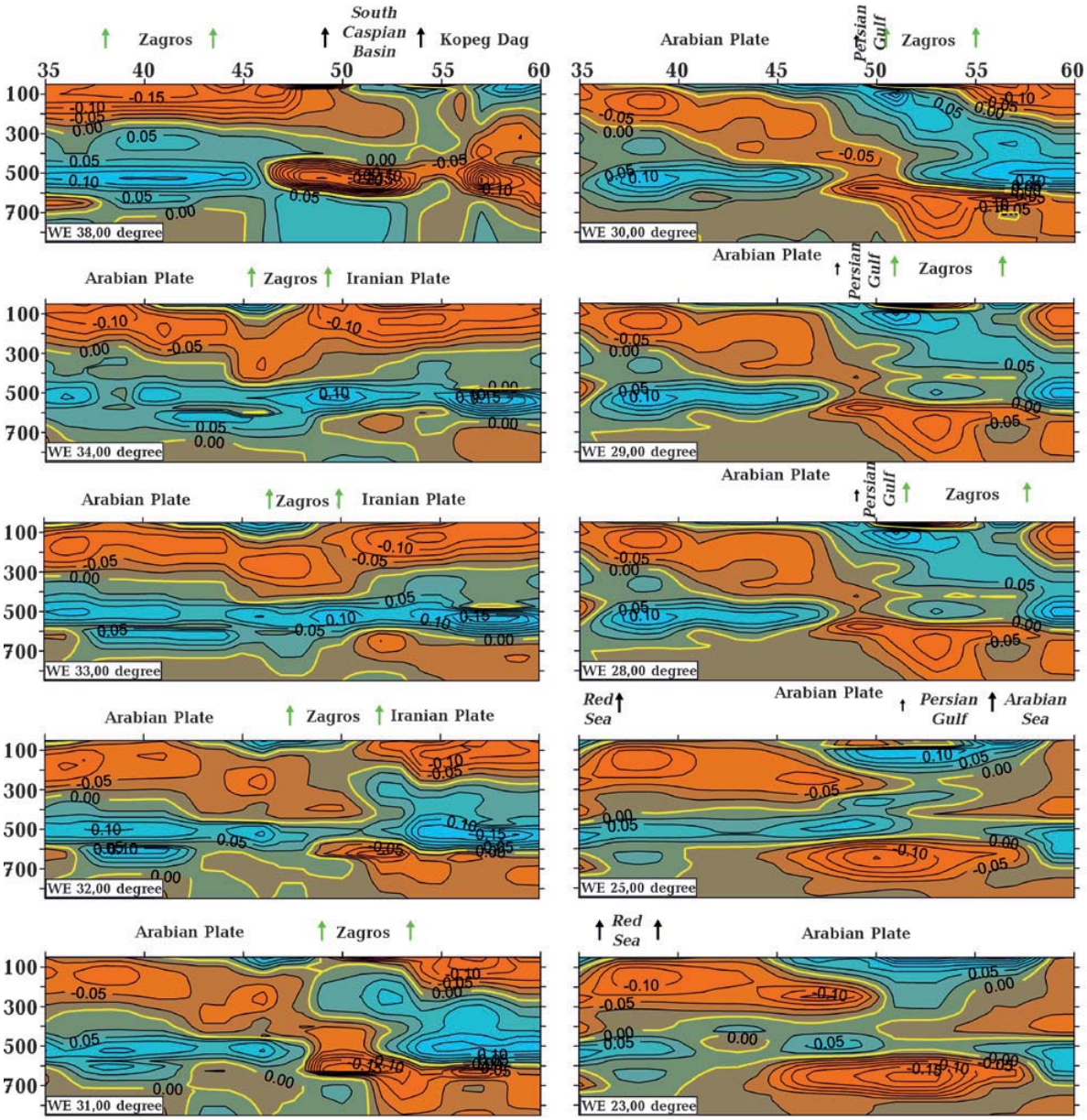

Fig. 10. Vertical latitudinal sections of the 3D *P*-velocity model of the mantle of the Zagros Folded Zone and its surroundings (38°, 34°, 33°, 32°, 31°, 30°, 29° 28°, 25°, 23° NL). Black arrows mark the boundaries of tectonic structures, green — Zagros.

thickness does not exceed 150 km. Evidently, the rest of the slab that lay above it was cut off during the horizontal movements within the frictional seismogenic zone of Zagros and adjacent areas (see Fig. 6).

On most vertical sections, the start-subduction areas lie at the SW margin of the Mesopotamian Valley and the Gulf of Persia, ~100—200 km beyond the Zagros foredeep and parallel to it. This is evidence of a close connection between the formation of the Zagros orogenic belt and the subduction processes recorded by seismotomography.

The reflection of the subduction process on the horizontal and vertical sections has a fairly complex character and cannot be unequivocally interpreted. Approximate determination of the slab's sinking direction by the data of longitudinal and latitudinal sections is possible by noting the points at which the slab passes the horizontal sections at different depths. To do this, one can use some structu-

ral elements of the slab, e.g., its upper or lower surface or the axial line. If the direction of the slab's sinking differs from the latitudinal or meridional, then at the horizontal section of a certain depth, the points of intersection found by the system of longitudinal and latitudinal profiles will lie on lines that would themselves diverge from the latitudinal and longitudinal, respectively. This is clearly seen in Fig. 11, compiled using this technique (using the slab's upper margin). The main difficulty in constructing the scheme lay in the relatively rare observation network (1°×1°) and, quite often, in the inability to determine the areas of high gradients of $\partial\delta/\partial xy$, which are commonly used to determine the contours of anomalous bodies (here, slabs). Besides that, the reconstructions were affected by slabs sinking from the East-European Platform.

Fig. 11 shows that the five latitudinal sections (28—32°NL) reflect the NE direction of the slab's sinking from 50 to 400 km. The sinking azimuth is from 30° to 45°. On ten longitudinal sections, the picture is more complicated: here, we can see areas of submeridional and NE directions of the slab's sinking. At the depths of 50—100 km, the areas of the beginning of the slab's sinking on the latitudinal and longitudinal sections are set apart. Thus, one can suppose that the northward subduction of the Arabian Plate on the side of the southern margin of the Gulf of Persia and the eastward subduction on the side of its SW margin are different processes. The submeridional sinking of the plate can be connected with the start of the northward submeridional movement of the plate in the Early Miocene (20 Ma). The NE sinking is typical for the Upper Cretaceous — Paleogene.

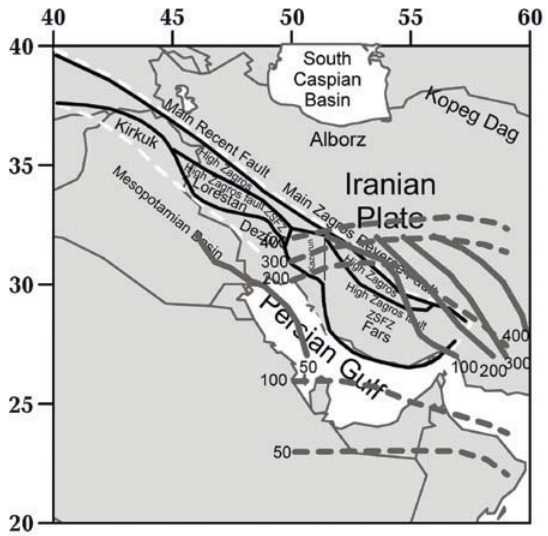

Fig. 11. Projections on the daytime surface of the lines of intersection of the horizontal planes 50, 100, 200, 300, and 400 km with the surface of the subducting Arabian Plate in longitudinal (gray dashed line) and latitudinal (gray line) sections of the 3D *P*-velocity model. Zagros Folded Zone is marked with discontinuous white lines.

However, the analysis of the subduction process can turn out to be much more complex if one supposes that all vertical sections reflect only the most recent (up to current times) process of subduction of the Arabian Plate under Zagros and the Iranian Plate. Then, one should suppose a very complex configuration of the slab in both projections or that it consists of several parts that move autonomously.

Another, possibly more probable explanation, was given above: the different directions of the subduction process (if it is continental and started in the Miocene) can be connected with the frequent alteration of the meridional and NE directions of the Arabian Plate's movement under the effect of the spreading processes in the Gulf of Aden and the SE part of the Red Sea.

Conclusions. The seismotomographic method of Taylor approximation allowed us to obtain images of the mantle of the whole of Eurasia and part of the African continent down to 850 km and over a significant area down to 2500 km. For the regions where we could compare them with the seismotomographic data of other authors, there were no substantial disagreements. We were able to study the deep structure of a number of regional Eurasian structures to which the Zagros belt belongs. Despite being well-studied from the points of view of geology and geophysics, the present seismotomographic materials allow us to put more or less trust into several principal statements set forth by previous studies and clarify some details of the paleotectonic reconstructions. We conclude the following.

1. To explain the Zagros Orogenic Belt's

formation is possible only by the plume-plate tectonical processes. The mountain system was formed due to plate tectonics starting in Early Paleozoic and still ongoing.

2. The main paleotectonic mechanisms of Zagros's formation are the subduction — collision and collision — slip fault. Of the 34 meridional and latitudinal sections of the three-dimensional model of Zagros, on 18 we found a high-velocity slab subducting under Zagros and the Iranian Plate from the south and south-west; it was the most clearly recognized on 15 latitudinal and longitudinal sections which cover the area of 23—32°NL — 49—58°EL (i.e., the Gulf of Persia, Central Zagros, and a significant part of the Iranian Plate).

The maximum horizontal length of the sinking part of the slab was 800—1100 km, and the maximum depth of sinking was 450—500 km. In the NW Zagros, the traces of subduction were less clear, yet the dextral deformations along MRF are distinct and ongoing.

3. The recorded inclined layer is a sank distal high-velocity part of the Arabian Plate, which separated off the African Platform in the Miocene-Pliocene and started migrating to NNE. Analysis of earthquake focuses of 1977—2001 showed that the migration could occur with the alternation of movements of the plate in the meridional and NE directions. The difference in the nature of the NE and Central Zagros deformation is most probably determined by the migrations and the specifics of the outlines of the eastern margin of the Arabian Plate.

4. Before the subduction of the Arabian Plate started, the oceans Paleo- and Neo-Tethys were formed to the east of it in the Middle-Late Paleozoic. Paleo-Tethys subducted under Eurasia at the end of the Mesozoic — the start of the Cenozoic (the collision process continues to the present) with the formation of disparate terrains of the Iranian Plate and its attachment to Eurasia. Neo-Tethys, located between the Arabian and the Iranian plates, subducted under the latter and closed off in the Paleocene; consequently, the Arabian Plate was joined to the Iranian. Thus, Zagros formation is a constant process of compression—dilation of the crust (with compression being more prevalent), which started at the end of the Mesozoic with the Neo-Tethys subducting under the Iranian Plate and is still ongoing as a result of collision compression.

5. Although the slabs considered in the paper reflect the continental subduction of the Arabian Plate under Zagros and the Iranian Plate, the traces of previous subduction processes of the oceanic lithosphere of Neo-Tethys could, in our view, be found as local high-velocity inhomogeneities on seismotomographic sections, complicating their interpretation.

References

Agard, P., Monié, P., Gerber, W., Omrani, J., Molinaro, M., Meyer, B., Labrousse, L., Vrielynck, B., Jolivet, L., & Yamato, P. (2006). Transient, synobduction exhumation of Zagros blueschists inferred from *P-T*, deformation, time, and kinematic constraints: implications for Neotethyan wedge dynamics. *Journal of Geophysical Research, 111*, B11401. https://doi.org/10.1029/2005JB004103.

Agard, P., Omrani, J., Jolivet, L., Whitechurch, H., Vrielynck, B., Spakman, W., & Wortel, R. (2011). Zagros orogeny: A subduction-dominated process. *Geological Magazine, 148*(5-6), 692—725. https://doi.org/10.1017/S001675681100046X.

Aki, K., Christoffersson, A., & Husebye, E.S. (1977). Determination of the three-dimensional seismic structure of the lithosphere. *Journal of Geophysical Research, 82*(2), 277—296. https://doi.org/10.1029/JB082i002p00277.

Alavi, M. (2007). Structures of the Zagros fold-thrust belt in Iran. *American Journal of Science*, *307*(9), 1064—1095. https://doi.org/10.2475/09.2007.02.

Alavi, M. (1994). Tectonics of Zagros orogenic Belt of Iran: new data and interpretation. *Tectonophysics, 229*(3-4), 211—238. https://doi.org/10.1016/0040-1951(94)90030-2.

Alinaghi, A., Koulakov, I., & Thybo, H. (2007). Seismic tomographic imaging of *P*- and *S*-waves

velocity perturbations in the upper mantle beneath Iran. *Geophysical Journal International, 169*(3), 1089—1102. https://doi.org/10.1111/j.1365-246X.2007.03317.x.

Allen, M. (2004). Late Cenozoic reorganization of the Arabia-Eurasia collision and the comparison of short-term and long-term deformation rates. *Tectonics, 23*, 1—16. https://doi.org/10.1029/2003TC001530.

Artemieva, I.M. (2009). The continental lithosphere: Reconciling thermal, seismic, and petrologic data. *Lithos, 109*, 23—46. https://doi.org/10.1016/j.lithos.2008.09.015.

Artemieva, I.M. (2019). The lithosphere structure of the European continent from thermal isostasy. *Earth-Science Reviews, 188*, 454—468. https://doi.org/10.1016/j.earscirev.2018.11.004.

Authemayou, C., Bellier, O., Chardon, D., Malekzade, Z., & Abbassi, M. (2005). Role of Kazerun fault system in active deformation of the Zagros fold-and-thrust belt (Iran). *Comptes Rendus Geoscience, 337*(5), 539—545. https://doi.org/10.1016/j.crte.2004.12.007.

Berberian, M. (1995). Master blind thrust faults hidden under the Zagros folds: active basement tectonics and surface morphotectonics. *Tectonophysics, 241*, 193—195, 197, 199—224. https://doi.org/10.1016/0040-1951(94)00185-C.

Berberian, M., & King, G. (1981). Towards a paleogeography and tectonic evolution of Iran. *Canadian Journal of Earth Sciences, 18*, 210—285. https://doi.org/10.1139/e81-019.

Bugaenko, I.V., Shumlyanskaya, L.A., Zaets, L.N., & Tsvetkova, T.A. (2012). Three-dimensional P-velocity model of the upper mantle of the Western Mediterranean. *Geofizicheskiy Zhurnal*, *34*(1), 14—31. https://doi.org/10.24028/gzh.0203-3100.v34i1.2012.116573 (in Russian).

Chang, S.-U., van der Lee, S., Flanagan, M.P., Bedle, H., Marone, F., Matzel, E.M., Pasyanos, M.E., Rodgers, A.J., Romanowicz, B., & Schmid, C. (2010). Joint inversion for three-dimensional S velocity mantle structure along the Tethyan margin. *Journal of Geophysical Research Atmospheres, 115*(B8), 1—22. https://doi.org/10.1029/2009JB007204.

Cocks, L.R.M., & Torsvik, T.H. (2006). European geography in a global context from the Vendian to the end of the Paleozoic (pp. 83—95). *Geol. Soc., London, Mem., 32*. https://doi.org/10.1144/GSL.MEM.2006.032.01.05.

Falcon, N.L. (1974). Southern Iran: Zagros Mountains. In A. Spencer (Ed.), *Mesozoic-Cenozoic Orogenic Belts, Data for Orogenic Studies: Alpine-Himalayan Orogens* (pp. 199—211). *Geol. Soc., London, Spec. Publ.*, No 4.

Geyko, V.S. (2004). A general theory of the seismic travel-time tomography. *Geofizicheskiy Zhurnal, 26*(1), 3—32.

Geyko, V.S. (1997). Taylor approximation of the wave equation and the eikonal equation in inverse seismic problems. *Geofizicheskiy Zhurnal, 19*(3), 48—68 (in Russian).

Geyko, V.S., Bugaenko, I.V., Shumlyanskaya, L.A., Zaets, L.N., & Tsvetkova, T.A. (2007). 3-D P-velocity structure of the upper mantle References of the Eastern Mediterranean. *Geofizicheskiy zhurnal, 29*(4), 13—30 (in Russian).

Geyko, V.S., Shumlyanskaya, L.A., Bugaenko, I.V., Zaets, L.N., & Tsvetkova, T.A. (2006). Three-dimensional model of the upper mantle of Ukraine by the terms of *P*-waves arrival. *Geofizicheskiy Zhurnal, 28*(1), 3—16 (in Russian).

Geyko, V.S., & Tsvetkova, T.A. (1989). On uniqueness in solution of unidimensional inverse kinematik problem of seismic. *Geofizicheskiy Zhurnal, 11*(6), 61—67 (in Russian).

Geyko, V.S., Tsvetkova, T.A., Sannikova, N.P., Livanova, L.P., & Geyko, K.V. (1998). Regional 3-D *P*-velocity structure of the mantle of northwestern Eurasia — I. Europe. 1. *Geofizicheskiy Zhurnal, 20*(3), 67—91 (in Russian).

Geyko, V.S., Tsvetkova, T.A., Shumlyanskaya, L.A., Bugaenko, I.V., & Zaets, L.N. (2005). Regional 3D *P*-velocity model of the Sarmatian mantle (south-west of the East European platform). *Geofizicheskiy Zhurnal, 27*(6), 927—939 (in Russian).

Gintov, O.B., Tsvetkova, T.A., Bugaenko, I.V., & Murovskaya, A.V. (2016). Some features of the structure of the mantle of the Eastern Mediterranean and their geodynamic interpretation. *Geofizicheskiy Zhurnal*, *38*(1), 17—29. https://doi.org/10.24028/gzh.0203-3100.v38i1.2016.107719 (in Russian).

Gintov, O.B., Tsvetkova, T.O., Bugaenko, I.V., Zayats, L.M., & Murovska, G.V. (2022). The

deep structure of the Trans-European Suture Zone (based on seismic survey and GSR data) and some insights in to its development. *Geofizicheskiy Zhurnal*, *44*(6), 63—87. https://doi.org/10.24028/gj.v44i6.273640 (in Ukrainian).

Golonka, J. (2004). Plate tectonic evolution of the southern margin of Eurasia in the Mesozoic and Cenozoic. *Tectonophysics, 381*, 235—273. https://doi.org/10.1016/j.tecto.2002.06.004.

Hafkenscheid, E., Wortel, M.J.R., & Spakman, W. (2006). Subduction history of the Tethyan region derived from seismic tomography and tectonic reconstructions. *Journal of Geophysical Research, 111*, 1—26. https://doi.org/10.1029/2005JB003791.

International Seismological Center. (2023). Retrieved from http://www.isc.ac.uk.

Jahani, S., Callot, J.-P., Letouzey, J., & de Lamotte, D.F. (2009). The eastern termination of the Zagros Fold-and-Thrust Belt, Iran: structures, evolution, and relationships between salt plugs, folding, and faulting. *Tectonics, 28*, TC600. https://doi.org/10.1029/2008TC002418.

Keshvari, E., Shomali, Z.H., Tatar, M., & Kaviani, A. (2011). Upper-mantle *S*-velocity structure across the Zagros collision zone resolved by nonlinear teleseismic tomography. *Journal of Seismology, 15*, 329—339. https://doi.org/10.1007/s10950-011-9226-y.

Khain, V.E. (2001). *Tectonics of continents and oceans*. Moscow: Nauchnyy Mir, 604 p. (in Russian).

Lacombe, O., Mouthereau, F., Kargar, S., & Meyer, B. (2006). Late Cenozoic and Modern Stress Fields in the Western Fars (Iran): Implication for the Tectonic and Kinematic Evolution of Central Zagros. *Tectonics, 25*, TC1003. https://doi.org/10.1029/2005tc001831.

Lavrentiev, M.M., & Romanov, V.G. (1966). About three linerarizing inverse problems for hyperbolic equations. *Doklady AN USSR, 171*, 1279—1281 (in Russian).

McQuarrie, N. (2004). Crustal-scale geometry of the Zagros fold-thrust belt, Iran. *Journal of Structural Geology, 26* (3), 519—535. https://doi.org/10.1016/j.jsg.2003.08.009.

Mouthereau, F., Lacombe, P., & Vergés, J. (2012). Building the Zagros collisional orogen: Timing, strain distribution and the dynamics of Arabia/Eurasia Plate convergence. *Tectonophysics, 532-535*, 27—60. https://doi.org/10.1016/j.tecto.2012.01.022.

Paul, A., Hatzfeld, D., Kaviani, A., Tatar, M., & Pequegnat, C. (2010). *Seismic imaging of the lithospheric structure of the Zagros mountain belt (Iran)* (Vol. 330, pp. 5—18). Geol. Soc., London, Spec. Publ. https://doi.org/10.1144/SP330.2.

Simmons, N.A., Myers, S.C., & Johannesson, G. (2011). Global-scale *P*-wave tomography optimized for prediction of teleseismic and regional travel times for Middle East events: 2. Tomographic inversion. *Journal of Geophysical Research, 116*, B04305. https://doi.org/10.1029/2010JB007969.

Shumlyanskaya, L.A., Tripolskiy, A.A., & Tsvetkova, T.A. (2014). Crustal velocity structure effects on the results of seismic tomography of the Ukrainian Shield. *Geofizicheskiy Zhurnal*, *36*(4), 95—117. https://doi.org/10.24028/gzh.0203-3100.v36i4.2014.116030 (in Russian).

Tsvetkova, T.A., & Bugaenko, I.V. (2016). The structure of velocity mantle number of horizons under Phennoscandia according to seismic-tomography data. *Geofizicheskiy Zhurnal*, *38*(1), 57—77. https://doi.org/10.24028/gzh.0203-3100.v38i1.2016.107723 (in Russian).

Tsvetkova, T.A., Bugaenko, I.V., & Zaets, L.N. (2020). Speed structure of the mantle under the Dnieper-Donets Depression and its surroundings. Part I. *Geofizicheskiy Zhurnal*, *42*(2), 71—85. https://doi.org/10.24028/gzh.0203-3100.v42i2.2020.201742 (in Russian).

Tsvetkova, T.A., Bugaenko, I.V., & Zaets, L.N. (2016). Velocity divisibility of the mantle beneath the Ukrainian shield. *Geofizicheskiy Zhurnal*, *38*(4), 75—87. https://doi.org/10.24028/gzh.0203-3100.v38i4.2016.107802 (in Russian).

Tsvetkova, T.A., Shumlyanskaya, L.A., Bugaenko, I.V., & Zaets, L.N. (2010). Seismotomography of the East European platform: a three-dimensional *P*-velocity model of the mantle near Fennoscandia. Part II. *Geofizicheskiy Zhurnal*, *32*(1), 60—77. https://doi.org/10.24028/gzh.0203-3100.v32i1.2010.117570 (in Russian).

Talebi, A., Koulakov, I., Moradi, A., Rahimi, H., & Gerya, T. (2020). Ongoing formation of felsic

lower crustal channel by relamination in Zagros collision zone revealed from regional tomography. *Scientific Reports, 10*, 8224. https://doi.org/10.1038/s41598-020-64946-w.

Talebian, M., & Jackson, J.A. (2004). A reappraisal of earthquake focal mechanisms and active shortening in the Zagros mountains of Iran. *Geophysical Journal International, 156*(3), 506—526. https://doi.org/10.1111/j.1365-246X.2004.02092.x.

Talebian, M., & Jackson, J. (2002). Offset on the Main Recent Fault of NW Iran and implications for the late Cenozoic tectonics of the Arabia-Eurasia collision zone. *Geophysical Journal International, 150*(2), 422—439. https://doi.org/10.1046/j.1365-246X.2002.01711.x.

Tavakoli, F., Walpersdorf, A., Authemayou, C., Nankali, H.R., Hatzfeld, D., Tatar, M., Djamou, Y., Nilforoushan, F., & Cotte, N. (2008). Distribution of the right-lateral strike—slip motion from the Main Recent Fault to the Kazerun Fault System (Zagros, Iran): Evidence from present-day GPS velocities. *Earth and Planetary Science. Letters, 275*(3-4), 342—347. https://doi.org/10.1016/j.epsl.2008.08.030.

Torsvik, T.H., Van der Voo, R., Preeden, U., Niocaill, C.M., Steinberger, B., Doubrovine, P.V., van Hinsbergen, D.J.J., Domeier, M., Gaina, C., Tohver, E., Meert, J.G., McCausland, P.J.A., & Cocks, L.R.M. (2012). Phanerozoic polar wander, palaeogeography and dynamics. *Earth-Science Reviews, 114*, 325—368. https://doi.org/10.1016/j.earscirev.2012.06.007.

Volfman,Y.M., Gintov, O.B., Kolesnikova, E.Ya., & Murovskaya, A.V. (2014). Tectonophysical interpretation of earthquake focal mechanisms of the Zagros system. *Geodynamics & Tectonophysics, 5*(1), 305—319. http://doi.org/10.5800/GT-2014-5-1-0129 (in Russian).

Wells, A.J. (1969). The Crush Zone of the Iranian Zagros Mountains, and its implications. *Geological magazine, 106*(5), 385—394. https://doi.org/10.1017/S0016756800058787.

Xu, Z., Dilek, Y., Cao, H., Yang, J., Robinson, P., Ma, C., Li, H., Jolivet, M., Roger, F., & Chen, X. (2015). Paleo-Tethyan Evolution of Tibet as Recorded in the East Cimmerides and West Cathaysides. *Journal of Asian Earth Sciences, 105*, 320—337. http://dx.doi.org/10.1016/j.jseaes.2015.01.021.

Zaets, L.N. (2011). Speed limits in the mantle of Southeast Asia and Southern China. *Geofizicheskiy Zhurnal*, *33*(1), 62—71. https://doi.org/10.24028/gzh.0203-3100.v33i1.2011.117326 (in Russian).

Zayets, L.N., Kao, D.T., & Tsvetkova, T.A. (2012). Velocity structure of the mantle and abyssal fluids of Southeast Asia. *Geofizicheskiy Zhurnal*, *34*(4), 108—127. https://doi.org/10.24028/gzh.0203-3100.v34i4.2012.116760 (in Russian).

Zaets, L.N., Tsvetkova, T.A., Bugaenko, I.V., & Shumlyanskaya, L.A. (2009). 3-D P-velocity structure of the upper mantle of Indochina and its surroundings. *Geofizicheskiy Zhurnal, 31*(2), 47—60 (in Russian).

Глибинна будова гірської системи Загрос за даними сейсмічної томографії методом тейлорового наближення

Т.О. Цвєткова, О.Б. Гінтов, І.В. Бугаєнко, Л.М. Заєць, 2023

Інститут геофізики ім. С.І.Субботіна НАН України, Київ, Україна

Розглянуто глибинну будову гірської системи Загрос в інтервалі глибин 50—850 км за допомогою сейсмічної томографії методом наближення Тейлора. Коротко схарактеризовано сам метод. На підставі структурно-геологічних і сейсмотомографічних матеріалів запропоновано двочленний поділ Загросу на Північно-Західний (області Кіркук, Лурестан і Дезфул) та Центральний (області Казерун і Фарс). Показано, що основними палеотектонічними механізмами формування Загросу є субдукційно-

колізійний (Центральний Загрос) і колізійно-зсувний (Північно-Західний Загрос). За матеріалами тривимірної *P*-швидкісної моделі мантії Загросу та його оточення встановлено високошвидкісну дистальну південно-східну частину Аравійської плити, що субдукує під Центральний Загрос та Іранську плиту, слідом за субдукцією Неотетісу. Цей слеб охоплює площу 23—32° пн.ш. — 49—58° сх.д., тобто Перську затоку, Центральний Загрос і значну частину Іранської плити. Максимальна горизонтальна протяжність частини Аравійського слебу, що занурюється, 800—1100 км, максимальна глибина занурення 450—500 км. За матеріалами вертикальних перетинів тривимірної моделі мантії побудовано проєкції на горизонтальну площину ліній перетину поверхні субдукуючої Аравійської плити з горизонтальними перетинами 50, 100, 200, 300 та 400 м. Це дало змогу визначити реальний напрямок занурення слебу, який на різних ділянках виявився або субмеридіональним, або північно-східним 30—45°. У Північно-Західному Загросі, за даними моделі, слідів субдукції не виявлено, проте чітко простежуються і продовжуються нині у корі правозсувні деформації вздовж Головного сучасного розлому. Відмінність у типах деформування Північно-Західного та Центрального Загросу обумовлена, найімовірніше, особливостями контурів східного краю Аравійської плити, а також складним характером її переміщень. Аналіз механізмів вогнищ землетрусів 1977—2001 років показав, що переміщення могло відбуватися з частим чергуванням рухів плити у субмеридіональному та північно-східному напрямках через чергування процесів спредінгу в Аденській затоці та у південно-східній частині Червоного моря.

Ключові слова: Загрос, Іранська плита, сейсмічна томографія, мантія, субдукція, колізія.